Integration of a Gas Switching Combustion (GSC) system in integrated gasification combined cycles

Schalk Cloete[a], Matteo C. Romano[b], Paolo Chiesa[b], Giovanni Lozza[b], Shahriar Amini[a,*]

[a] *SINTEF Materials and Chemistry, Trondheim, Norway*
[b] *Department of Energy, Politecnico di Milano, Milan, Italy*

Received 14 July 2015
Received in revised form 7 August 2015
Accepted 14 August 2015
Available online 2 September 2015

1. Introduction

Chemical Looping Combustion (CLC) is one of the most promising technologies for CO_2 capture from gas and coal fed power plants (Adanez et al., 2012). This process performs an indirect oxidation of the fuel by means of an oxygen carrier, which is sequentially reduced and oxidized by the contact with fuel and air respectively. The most attractive characteristic of CLC technology is the intrinsic generation of a concentrated CO_2 stream from fuel oxidation undiluted with air N_2 as in oxyfuel combustion plants, but with no need of high cost and high electric consumption cryogenic air separation unit (ASU). Extensive theoretical and experimental research has been carried out in the last 10–15 years on the application of CLC process on gaseous fuels, which led to the demonstration of the process by different research groups worldwide (Adanez et al., 2012). More recently, the direct utilization of solid fuels gained a great interest and was also tested at lab scale (Lyngfelt, 2014).

Different configurations have been proposed in the literature for the CLC reactor system operated with gaseous fuels. Most of the theoretical and experimental research up to now has been devoted to interconnected dual fluidized bed systems. The integration of such a system in power plants has been assessed in a number of process simulation studies showing the potential of achieving high efficiencies and near-zero CO_2 emissions (Brandvoll and Bolland, 2004; Consonni et al., 2006; Cormos, 2010; Erlach et al., 2011; Lozza et al., 2006; Naqvi and Bolland, 2007; Naqvi et al., 2007; Sorgenfrei and Tsatsaronis, 2014; Wolf et al., 2005). However, for power gen-eration from gaseous fuels, the CLC reactors need to operate at high pressure and high temperature. As a matter of fact, only high pressure operations allow feeding a gas turbine and obtaining elec-tric efficiencies in line with competitive technologies, which are all based on gas–steam combined cycles.

Interconnected dual fluidized bed systems have thus far not been demonstrated under high pressure operation (10–30 bar) due to well-known technical challenges related to the achievement of

* Corresponding author at: Department of Flow Technology, SINTEF Materials and Chemistry, S.P. Andersens vei 15 B, 7031 Trondheim, Norway.
E-mail address: shahriar.amini@sintef.no (S. Amini).

List of symbols

α	volume fraction
$\Delta H_{reaction,298\,K}$	enthalpy of reaction at 298 K (J/mol)
η_{el}	electric LHV efficiency
C	molar concentration (mol/m^3)
C_p	specific heat capacity (J/(kg K))
c_p	molar heat capacity (J/(mol K))
d	diameter (m)
E_{CO_2}	specific CO_2 emissions (g/kW h)
H	enthalpy (J)
HE	Heat exchanger
HP/IP/LP	high/intermediate/low pressure
HRSG	heat recovery steam generator
k	reaction rate constant
LHV	lower heating value
N	number of moles (mol)
$\dot{N}$	molar flow rate (mol/s)
n	reaction order
P	pressure (Pa)
R	universal gas constant (8.314 J/(K mol))
R_H	heterogeneous reaction rate (mol/(m^3 s))
S_T	turbine nozzle area
s	ratio of unreacted core surface area to grain surface area
SPECCA	specific primary energy consumption for CO_2 avoided
T	temperature (K)
TV	throttling valve
t	time (s)
U	velocity (m/s)
V	volume (m^3)
x	distance along reactor height (m)
y	species mole fraction

Subscripts

ADV	advanced gas turbine technology
CUR	current gas turbine technology
eff	effective
g	gas
gr	grain
i	species index
mf	minimum fluidization
ref	reference plant

stable solid circulation between the two fluidized bed reactors at high pressure. Another technical issue is related to the need for a high pressure and high temperature filtering system to avoid entrainment of solid particles to the turbine, which may damage the machine.

Another possible reactor configuration for CLC, which is gaining increasing interest more recently, is the packed bed (PB) system (Hamers et al., 2013; Noorman et al., 2011b; Spallina et al., 2013). The main advantage over fluidized beds is that the need for solid circulation between pressurized reactors is avoided in this case, since the oxygen carrier always remains in the same vessel, which is sequentially fed with air and fuel by means of a switching valve system.

In addition, if an oxygen carrier with proper mechanical resistance to thermal and chemical stresses can be selected so that no fines are formed during normal operations, high pressure and high temperature filtration can be avoided in this case. On the other hand, a high temperature switching valve system and a series of parallel reactors are needed, which make the system more complex. In addition, heat management is more complicated in this case. Steep temperature gradients occur in packed bed reactors due to the establishment of reaction and heat fronts. Therefore, proper operation strategies are needed to produce a flow with a temperature sufficiently stable to feed a gas turbine.

This concept has been demonstrated at lab-scale tests in heated reactors (Noorman et al., 2011a). Modelling works also explored and compared different operation strategies, anticipating the possibility of generating gas streams with sufficiently stable temperature in adiabatic reactors with different oxygen carriers (Noorman et al., 2011b; Spallina et al., 2013) or by combining two oxygen carriers in the same bed (Hamers et al., 2013). Process simulation studies finally assessed the application of PB-based CLC systems in integrated gasification CLC (IGCLC) plants, showing a high potential of this option in terms of both electric efficiency and CO_2 emission (Hamers et al., 2014, 2015; Spallina et al., 2014), indicating a limited expected difference with respect to fluidized bed systems (Hamers et al., 2014).

More recently, a third option for CLC reactor configuration, based on a rotating reactor, has been proposed (Håkonsen and Blom, 2011; Håkonsen et al., 2014). In this case, the metal oxide is kept in a doughnut-shaped fixed bed that rotates between two sections where it is contacted with the different gas streams flowing radially outward through the bed. In this case, solid circulation, high temperature gas filtering and high temperature valve system are avoided. On the other hand, relevant gas leakages leading to low CO_2 capture efficiencies and/or low CO_2 purity have been observed from the first experimental tests. However, the experimental tests performed up to now are limited and it is likely that improved per-formance can be achieved after improvement of the reactor design. A fourth option has been recently proposed, based on the Gas Switching Combustion (GSC) concept (Zaabout et al., 2013). In this case, the CLC process is based on a series of non-interconnected fluidized beds sequentially exposed to air and fuel streams. As in packed bed systems, no solids circulation between pressurized reactors is needed in this case. At the same time, uniform tempera-tures can be kept inside the reactors, making the heat management simpler. Good mixing in the reactors also negates the need for fuel dilution to avoid carbon deposition and over-reduction of the oxy-gen carrier since the maximum degree of reduction of the oxygen carrier can be controlled. Significant efficiency penalties are asso-ciated with fuel dilution, especially when steam from the steam cycle is used (Spallina et al., 2014). On the other hand, the good gas mixing in the fluidized bed reactors will lead to more undesired gas mixing after a switch in the feed gasses is made, leading to lower CO_2 capture ratio and lower CO_2 purity or requiring larger steam consumptions for purging between oxidation and reduction stages. A high temperature valve system and high temperature filtering are also needed in this case.

However, the most important advantage of the fluidized bed GSC concept over the packed bed is that material-related challenges will be greatly reduced. Material development is the primary chal-lenge hampering the progress of CLC systems (Adanez et al., 2012) and any concept capable of minimizing this challenge automatically appears highly promising.

The packed bed concept introduces new material-related challenges because it requires raw material to be shaped into pellets which must display sufficient strength and reactivity in order to function reliably over many cycles. Recent work examining several different ilmenite-based materials has shown that only one material with Mn_2O_3 as additive displayed promising mechanical properties (Ortiz et al., 2014). In addition, in the packed bed concept the reactor inlet is at a relatively low-temperature when reduction begins, since it is cooled to the temperature of the GT compressor outlet during the previous oxidation or heat removal phase. There-fore, low-temperature reduction with syngas towards the start of the reactor is required unless the more complex solution of feeding

air and fuel from opposite sides of the reactor is implemented as described in the counter-current configuration in Spallina et al. (2014) or a two-stage system is employed (Hamers et al., 2015).

Initial modelling studies showed that complete conversion can be achieved in the packed bed reactor even using the simplest configuration (Spallina et al., 2013). These results might be optimistic, however, as kinetics determined for ilmenite powder between 800 and 950 °C at atmospheric pressure (Abad et al., 2011) were used to simulate a packed bed reactor with ilmenite pellets operating between 400 and 1200 °C at 20 bar. Firstly, conversion at temperatures as low as 400–450 °C should be confirmed, since extrapolation of kinetics determined at 800–950 °C might not be representative under these conditions. Secondly, the effect of intra-particle mass transfer should be further investigated, especially if fast kinetics is used in pressurized systems. And thirdly, it is possible that kinet-ics at 20 bar is substantially slower than kinetics at atmospheric pressure based on high pressure TGA experiments performed on an Fe-based oxygen carrier material (Abad et al., 2007).

Three more generic material-related advantages of the fluidized bed over the packed bed can also be identified. Firstly, no special-ized material manufacturing is required as in the case of the packed bed system as very cheap raw ilmenite ore can be used directly in the reactor (Cuadrat et al., 2012). Secondly, continuous replenish-ment of spent material should be possible as opposed to the packed bed which will have to be taken offline and reloaded when the oxygen carrier material is spent. And thirdly, since fresh ilmenite shows poor reactivity before it has been activated over a number of cycles (Adanez et al., 2010), the packed bed reactor will require a special material activation procedure each time that the reactor is reloaded with fresh material (or the material must be pre-activated outside of the reactor at a significant cost). In contrast, the well-mixed GSC reactors can be initially started up with only a small fraction of preactivated material in a bed of fresh material and fresh material can continuously be used to replenish spent material to be activated in situ through the high temperatures present throughout the reactor.

Due to these advantages, this work has been conducted to assess the integration of the GSC reactor system in a complete power plant based on coal gasification. On one hand, different reactor operating modes are assessed and compared, discussing their suitability for application in a GT-based power cycle. Particular attention is given to the effects of the different operation strategies on the variability of the hot gas temperature, to CO_2 capture ratio and CO_2
purity. On the other hand, the results of the complete IGCLC power plant process simulations are presented, discussing the potential of this system in terms of net electric efficiency and CO_2 capture ratio achievable. Process simulations are carried out with assumptions coherent with previous or parallel studies of the authors of this paper on PB and FB-based IGCLC plants (Hamers et al., 2014; Spallina et al., 2014), allowing a direct comparison of the results among these studies.

2. Reactor simulations

The GSC cycle was simulated via a Continuous Stirred-Tank Reactor (CSTR) model where perfect mixing is assumed. This assumption should be reasonably accurate in the well-mixed fluidized beds used in the GSC concept.

2.1. Model equations

The mole and energy balances solved by the CSTR model will be described in this section. Individual mole balances were carried out for each species as follows:

$$\frac{dN_i}{dt} = \dot{N}_{i,in} - \dot{N}_{i,out} + \dot{N}_{i,reaction} \quad (1)$$

The reaction term ($\dot{N}_{i,reaction}$) was calculated under the assumption that the three reactions below occur instantaneously whenever all the reactants are present. The validity of this assumption of complete reactant conversion is verified in Appendix.

$$H_2 + Fe_2O_3 \rightarrow 2FeO + H_2O$$

$$CO + Fe_2O_3 \rightarrow 2FeO + CO_2$$

$$O_2 + 4FeO \rightarrow 2Fe_2O_3$$

The outflow rates ($\dot{N}_{i,out}$) in Eq. (1) were calculated by solving an overall mole balance of all the gaseous species passing through the reactor (Eq. (2)). The effect of transient temperature variations on the accumulation term was calculated via the ideal gas equation of state given the constant gaseous volume in the reactor.

$$\dot{N}_{i,out} = y_i \left(\dot{N}_{in} + \dot{N}_{reaction} + \frac{PV}{RT^2}\frac{dT}{dt} \right) \quad (2)$$

The mole fraction at the reactor outlet (y_i) was assumed equal to the mole fraction in the perfectly mixed CSTR.

Energy conservation was carried out as follows:

$$\frac{dH}{dt} = \sum_{i=1}^{n} \left(\dot{N}_{i,in} \int_{298}^{T_{in}} c_{p,i} dT \right) - \sum_{i=1}^{n} \left(\dot{N}_{i,out} \int_{298}^{T_{out}} c_{p,i} dT \right) - \sum \dot{N}_{reactant} \Delta H_{reaction,298\,K} \quad (3)$$

On the right hand side of Eq. (3), the first two terms represent the energy extraction from heating up the gasses passing through the reactor, the third term represents the enthalpy of reaction (highly exothermic for oxidation and slightly endothermic for reduction), and the last term represents the losses from the pressure drop over the bed.

The rate of enthalpy change (left hand term in Eq. (3)) manifests a temperature change in all the material present inside the reactor, thus resulting in the energy balance in Eq. (4).

$$\sum_{i=1}^{n} \left(N_i c_{p,i} \frac{dT}{dt} \right) = \sum_{i=1}^{n} \left(\dot{N}_{i,in} \int_{298}^{T_{in}} c_{p,i} dT \right) - \sum_{i=1}^{n} \left(\dot{N}_{i,out} \int_{298}^{T_{out}} c_{p,i} dT \right) - \sum \dot{N}_{reactant} \Delta H_{reaction,298\,K} \quad (4)$$

2.2. Geometry, boundary conditions and materials

The simulated reactor was 12 m in height and 7 m in diame-ter. The average solids volume fraction in the reactor was taken as 0.35 (creating a static bed height of 7 m at a solids volume frac-tion of 0.6). Such a tall bed was selected to increase the validity of the assumption of complete reactant conversion under the short residence times and large bubbles created by fairly vigorous fluidization conditions (10–20 times U_{mf} if 200–250 μm particles are used). A relatively high fluidization velocity was required to ensure a reasonable reactor diameter. Vigorous fluidization would also ensure validity of the assumption of perfect mixing in the reactor.

Inlet boundary conditions are given in Table 1. The case depend-ent variables in Table 1 were generally determined as follows: the fuel stage time would be changed to adjust the degree of oxy-gen carrier conversion desired (longer fuel times would result in a higher degree of oxygen carrier reduction), the air stage time would be a certain integer multiple of the fuel stage time (mostly 7 times larger) in order to treat the simulation as part of a cluster of reactors, and the air flow rate would be fine-tuned to achieve a maximum temperature of 1200 °C in each run.

Table 1
Gas inlet conditions.

Stage	Time (s)	Flow rate (kg/s)	Temperature (°C)	Composition (mole fraction)	
Fuel	Case dependent	72.27 (unless otherwise specified)	300	H_2	0.2312
				CO	0.5677
				H_2O	0.0852
				CO_2	0.0933
				Ar	0.0098
				N_2	0.0128
Air	Case dependent	Case dependent	435	H_2O	0.0103
				CO_2	0.0003
				O_2	0.2073
				Ar	0.0092
				N_2	0.7729

The oxygen carrier density was taken as 4000 kg/m^3 (typical value for ilmenite ore) and was simulated to consist only of Fe_2O_3, FeO and TiO_2. In the fully oxidized state, 33% (weight) of the particle was composed of Fe_2O_3 with the remainder being TiO_2. Temperature dependent thermodynamic data was taken from Robie and Hemingway (1995) for the solids and the JANAF thermochemical tables (Stull and Prophet, 1971) for the gas.

No pressure drop was considered over the distributor under the assumption that this is small enough to be neglected at this stage of the investigation into the GSC concept. A review of studies on the required distributor pressure drop conducted by Kunii and Levenspiel (1991) yielded a broad range of recommendations ranging from 1.5% to 40% of the overall bed pressure drop. The required distributor pressure drop decreases substantially with increasing fluidization velocity though. For example, the lower-bound rec-ommendation of 1.5% of overall bed pressure drop is valid for fluidization velocities much greater than $2U_{mf}$ (Hiby, 1964). For fluidization velocities below $2U_{mf}$, the recommended distributor pressure drop is 15% in the same study. The vigorous fluidization employed in this study should therefore allow for the use of a rel-atively small distributor pressure drop without compromising the quality of fluidization.

It should also be mentioned that no inflow or outflow of solids is considered in this study. In reality, some flowrate of hot solids will leave the reactor to be replenished by cold material, thus leading to some degree of thermodynamic efficiency loss in the overall plant. Here we assume a good oxygen carrier material which remains active in the reactor for hundreds of cycles, thereby making this effect negligibly small.

2.3. Solver settings

The CSTR model was solved iteratively at each timestep using Visual Basic in MS Excel. Model testing revealed that a high level of numerical accuracy could be achieved when 1 s timesteps were employed.

2.4. Operation and data extraction

The model returned transient reactor outlet profiles of temperature, mass flow rate and gas composition. These data were processed to deliver the average temperature, mass flow rate and composition of both the CO_2-rich and depleted air outlet streams to the power-plant simulation. The average temperature was determined by means of a weighted average as follows: $T_{ave} = \dot{m}C_pT/\quad \dot{m}C_p$.

3. Integration of GSC process in a complete power plant

The configuration of the complete power plant based on the GSC process assessed in this work is shown in Fig. 1.

Coal gasification is performed by means of the Shell gasification process, which has been described more in detail in previous works (Spallina et al., 2014). South African Douglas Premium bituminous coal is loaded with high pressure CO_2, taken from the final CO_2 compression section. CO_2 is used here instead of N_2 typically employed in dry-feed gasifiers in order to avoid excessive dilution of the final CO_2. Coal is gasified with a 95 vol.% pure O_2 stream produced by a stand-alone cryogenic air separation unit (ASU) based on a double reboiler LP column and pumped liquid oxygen process (IEA, 2005). Part of the IP steam generated in the gasifier membrane walls is also injected in the gasifier as temperature moderator. Syn-gas produced in the gasifier is quenched to 900 °C with recycled low temperature syngas, allowing for the complete solidification of the ash. Afterwards, syngas is cooled in convective syngas coolers by producing high pressure moderately superheated steam at 400 °C and high pressure saturated water.

After the first cooling section, syngas is filtered in candle filters and scrubbed to remove the remaining fines and absorb the soluble contaminants. Syngas is then slightly reheated and sent to a catalytic COS hydrolyser, where all the sulfur is converted into H_2S. Syngas is then cooled in the low temperature heat recovery section, where low temperature water is produced for different uses in the plant (water for syngas saturator, scrubber water heater, steam cycle water economizer). After a final cooling by cooling water, H_2S is removed by Selexol physical absorption process. Cleaned syngas from AGR unit is then heated up and moisturized in a saturator and then heated up to 300 °C with heat from raw syngas cooling. Preheated syngas is then fed to the GSC unit where it is oxidized by the OC. It must be highlighted that, differently form packed bed CLC systems, after the saturator no further dilution with steam or recycled CO_2/H_2O is performed in this case. As a matter of fact, the intense mixing obtained in fluidized beds leads to good availability of oxidized OC in the entire volume of the reactor, capable of releasing oxygen in reducing atmospheres reducing in this way the risk of C deposition.

The generated CO_2/H_2O stream is then cooled down to nearly ambient temperature by raising high pressure steam, by producing HP saturated water and by further cooling by cooling water. CO_2-rich stream is then sent to the CO_2 purification unit (CPU), where CO_2 is purified according to the specifications of the transport pipeline and the storage site. In this study, a CO_2 content of around 96 mol.% has been assumed. This purification step is needed because of the relatively low purity of the CO_2 stream from the GSC process. Impurities are due to the presence of non-condensable species in the syngas, deriving from both nitrogen in the coal and from the non-perfect purity of the O_2 produced in the ASU, and above all to N_2 and O_2 leakages occurring in the GSC system when switching from the air to the fuel stage. Therefore, finding oper-ating conditions minimizing leakages of non-condensable gases to the CO_2 stream is a primary objective of GSC process optimization. CO_2 purification is based on the auto-refrigerated dual-flash process shown in Fig. 2, similar to the one presented in Chiesa

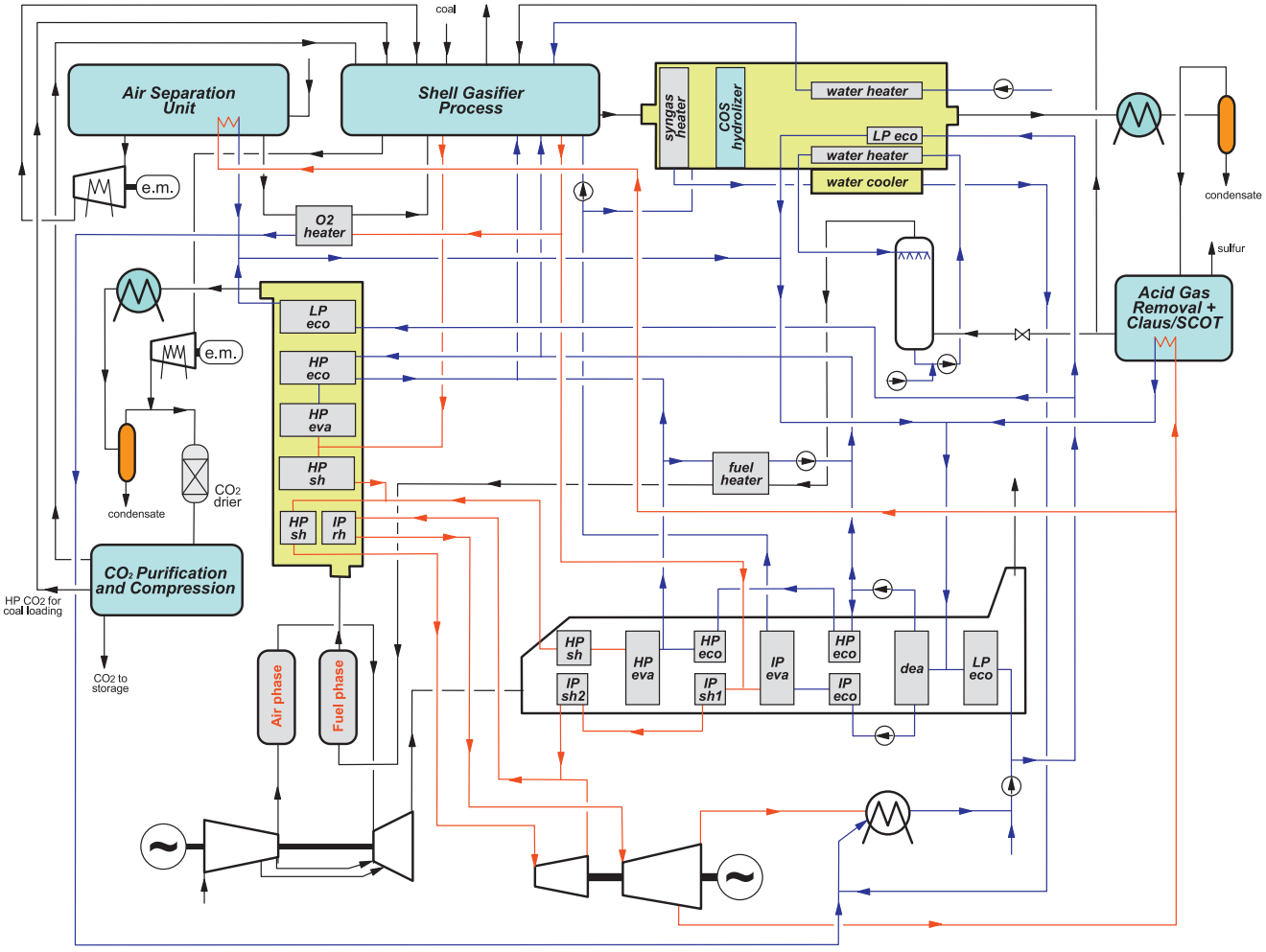

Fig. 1. Configuration of the base IGCLC plant based on GSC process assessed in this work.

et al. (2011). The cooled CO_2 from the CLC reactors is pressurized to 25.8 bar, mixed with the recycled CO_2 recovered from the lock hopper system and sent to the drying section, where water is completely adsorbed to avoid solids formation in the downstream low temperature section. CO_2 is then cooled to −33 °C in a multi-flow heat exchanger and sent to the first flash vessel where a first separation between a rich-CO_2 liquid and a vapor containing most of the non-condensable gases is performed. This vapor is then

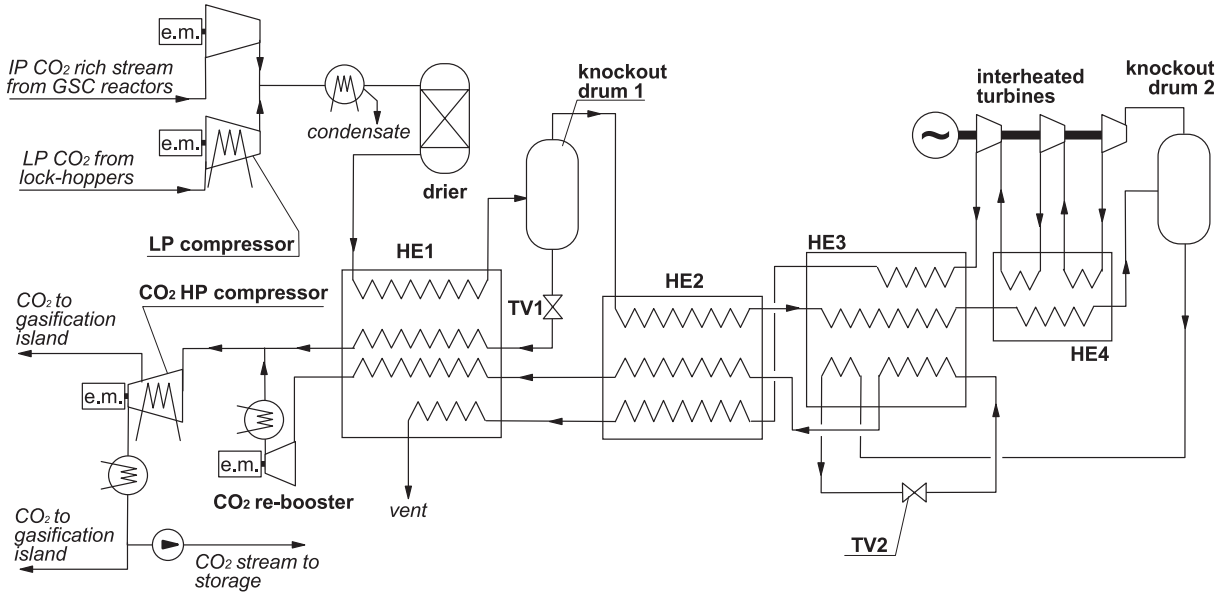

Fig. 2. Schematic of the CO_2 purification and compression unit (HE, heat exchanger; TV, throttling valve).

further cooled down to −54 °C in another multi-flow heat exchanger and sent to the second flash vessel. Vapor released from the second flash is expanded to nearly ambient temperature in a low temperature three-stage inter-heated expander, producing chilling power for impure CO_2 stream cooling and some electric power. Liquid stream from the two flash vessels is also throttled to produce chilling power and provide the required ΔT in the heat exchangers. The purified CO_2 streams, re-evaporated in the heat exchangers, are compressed to the pressure of 88 bar, condensed and pumped to the final pressure of 150 bar. During the compression process, part of the CO_2 is extracted at 56 and 88 bar to be used in the gasification island for coal loading and candle filters cleaning. The power island of this IGCLC plant is based on a gas–steam combined cycle. Similarly to all the pressurized CLC systems, GSC process is fed with a compressed air stream and releases a hot O_2-depleted air stream which is expanded in the gas turbine. In other words, the air reactor of the GSC replaces the combustor of the gas turbine. Expanded gas is then cooled in a heat recovery steam generator and then vented to the atmosphere. Also in this case, CO_2 leakages to the air flow occur when switching from the fuel to the air stage. This leakage has the effect of reducing the CO_2 capture efficiency of the plant, since it is eventually vented to the atmosphere with the O_2-depleted air.

The bottoming heat recovery steam cycle is based on a three pressure level (170/36/4 bar) Rankine cycle with reheat. Heat is recovered from GT flue gas, CO_2/H_2O stream cooling and syngas coolers. Final superheating and reheating up to 565 °C are carried out with the CO_2/H_2O stream. As a matter of fact, gas turbine outlet temperature is not high enough to achieve the selected maximum steam temperature, typical of large state-of-the-art heat recov-ery steam cycles. Therefore, the moderately superheated HP and IP steam produced from syngas and GT flue gas cooling is finally superheated with the high temperature CO_2/H_2O stream.

In addition to this basic configuration of the power island, more sophisticated cases have been considered, where part of the N_2-rich gas at HRSG outlet is recycled at compressor inlet so as to reduce the oxygen concentration in the air stream sent to the GSC process. The increased inert content allows reducing the temperature increase during the oxidation step, increasing in this way the average turbine inlet temperature and the cycle efficiency. Additional details on the GSC system operations under these conditions are described in the following.

The main assumptions used for the simulations are resumed in Table 2. These assumptions are coherent with those used in Hamers et al. (2014) and Spallina et al. (2014) and are mainly taken from the EBTF document (EBTF, 2011), properly adapted when needed after discussion with the industrial partners of the EU-funded DemoCLOCK project (DemoCLOCK, 2011). Process simulations are performed with the GS code (Gecos, 2014), except for CO_2 compression and purification unit, which is calculated with Aspen Plus utilizing the Peng Robinson equation of state with default coefficients.

3.1. Integrating the GSC process in a gas turbine power cycle

A significant issue to discuss for the integration of the GSC process in a combined cycle is related to the requirements for the stream to be expanded in the gas turbine, which are particularly stringent. First of all, gas expanded in the turbine needs to be virtually free of entrained particles, which may erode the blades surface and block the cooling channels. This requires a deep filtration of the hot air stream before expansion. In addition, temperature and mass flow rate has to be as stable as possible. To explain the effect of temperature and mass flow rate variations, it can be recalled that industrial gas turbines characteristic curve is typically governed by the fluid dynamics of the first nozzle, which operates under chocked conditions. This means that under operations with ideal gases of given composition, the dimensionless mass flow rate $\dot{m}_R$ keeps constant for a given geometry (Eq. (5), where temperature, pressure and flow rate refer to the conditions at the inlet of the turbine with nozzle area S_T).

$$\dot{m}_R = \frac{\dot{m}\sqrt{RT}}{p \cdot S_T} = constant \tag{5}$$

Therefore, variations of mass flow rate and temperature of the inlet gas lead to corresponding variations of the inlet pressure (proportionally to the variations of the mass flow rate and of the square root of the temperature in K), which can affect the mechanical resistance of the upstream equipment, of the gas turbine bearings (which should be properly sized) and could lead to unstable compressor operations. In addition, temperature variations induce thermal fatigue phenomena, which reduce the life of the components exposed to temperature gradients (in particular the first turbine nozzle, in this case).

Other requirements to achieve good efficiency of the gas turbine are related to the Δp between the air compressor outlet and the turbine inlet, which should be the lowest possible, and to the turbine inlet temperature, which should be the highest possible compatibly with the materials and the cooling technology of the turbine. All these points should be considered when evaluating the integration of the GSC process with a gas turbine and will be discussed in the sensitivity analysis presented in the following sections.

4. Results and discussion

Results will be presented in five main sections. In the first section, the effect of changing the fuel feed rate in order to adjust the number of reactors required will be investigated. Secondly, the degree of oxygen carrier utilization will be changed to increase the cycle time and improve CO_2 separation efficiency. Thirdly, a steam purge stage will be inserted between the fuel and air stages in order to reduce mixing of CO_2 and N_2. Fourthly, advanced heat management strategies using an N_2 recycle stream will be investigated. Finally, results are summarized and compared to an IGCC plant with standard CO_2 capture technology.

4.1. Effect of fuel feed rate

Three cases were completed under operating conditions as given in Table 1. Case A1 was designed for a cluster of 8 reactors (1 in reduction and 7 in oxidation/heat removal), Case A2 for a cluster of 4 reactors and Case A3 for a cluster of only 2 reactors.

Case A1 requires the largest number of reactors in the cluster, but will exhibit better reactor utilization. For example, the 8 reactors achieve a consistent fuel throughput of 72.27 kg/s, while Case A3 achieves a 7 times lower fuel throughput using 2 reactors. Therefore, 7 clusters operating according to Case A3 (14 reactors in total) will be required to achieve the same throughput as the 8 reactors of Case A1.

More importantly, however, outlet streams from the large num-ber of reactors under oxidation can be mixed before being sent to the turbine in order to minimize the overall fluctuations in mass flow rate and temperature. This is important because, as can be seen in Fig. 3, the outlet mass flow rate and temperature from each single reactor outlet stream vary substantially over one cycle.

As shown in Fig. 3, the fuel stage cools the reactor due to the heat extracted by the gas and the slightly endothermic reaction. The mass flow rate at the outlet also increases as denser CO_2 displaces lighter N_2 at the outlet. As the air stage begins, the outlet temperature starts to increase rapidly due to the highly exothermic oxidation reaction. The mass flow rate also drops because 23% of the mass in the air stream (O_2) is consumed in the oxidation

Table 2
Main assumptions for the calculation of the IGCLC power plant.

Bituminous South African Coal (composition and heating values)	
Composition, wt.%: C 66.52 (fixed C 54.9%); N 1.56; H 3.78; S 0.52; O 5.46, Ash 14.15; Moisture 8. LHV: 25.02 MJ/kg; HHV: 26.04 MJ/kg	
Gasification and coal pre-treating unit	
Gasification pressure, bar	44
Oxygen to carbon ratio, kg_{O_2}/kg_{coal}	0.903
Heat losses in gasifier, % of input LHV	0.7
H_2O in coal after drying, wt.%	2
Fixed carbon conversion, %	99.3
Moderator steam, $kg_{H_2O_2}/kg_{coal}$	0.09
Moderator steam pressure, bar	54
Temperature of O_2 to gasifier, °C	180
Heat to membrane walls, % of input coal LHV	2
Coal milling and handling, kJ_e/kg_{coal}	50
Slag handling, kJ_e/kg_{ash}	100
Syngas quench	
Quenched syngas temperature, °C	900
Cold recycled syngas temp, °C	300
Recycle compressor polytropic efficiency, %	75
Recycle compressor el./mech. efficiency, %	92
CO_2 operated lock hoppers	
VHP/HP CO_2 pressure, bar	88/56
CO_2 temperature, °C	80
CO_2 consumption, $kg_{CO_2}/kg_{dry\text{-}coal}$	0.826
CO_2 not recovered for CCS, % of CO_2 inlet flow rate	10
Air separation unit	
Oxygen purity, mol.%	95
Pressure of delivered oxygen, bar	48
Pressure of delivered nitrogen, bar	1.2
Temperature of delivered O_2 and N_2, °C	22
Electric consumption, kWh_e/t_{O_2}	325
LP steam heat rate for TSA beds regeneration, kWh_{th}/t_{O_2}	58.3
Heat exchangers	
Minimum ΔT in gas–liquid, liquid–liquid, gas-evaporating fluid heat exchangers, °C	10
Minimum ΔT in gas–gas and gas–steam heat exchangers, °C	25
Heat losses, % of heat transferred	0.7
Maximum steam T in the syngas coolers, °C	400
Acid gas removal (Selexol process)	
Syngas temperature at absorption tower inlet, °C	35
Syngas pressure loss, % of inlet pressure	1
LP steam heat rate, MJ_{th}/kg_{H_2S}	20.95
Electric consumption for auxiliaries, MJ_e/kg_{H_2S}	1.93
Gas turbine	
Compressor pressure ratio	20.0
Maximum compressor polytropic efficiency,[a] %	92.5
Maximum efficiency of large turbine stages (cooled/uncooled),[a] %	92.1/93.1
Mechanical efficiency of each turbomachine, %	99.865
Gas turbine auxiliary consumption, % of net mechanical power	0.35
Electric generator efficiency, %	98.7
Pressure drops	
Syngas pressure drop between gasifier and AGR, % of gasifier outlet pressure	12
Gas side pressure drop in HRSG, kPa	3
Pressure drop for CO_2/H_2O stream cooling, % of GSC reactor outlet pressure	6
Heat recovery steam cycle	
Pressure levels, bar	170/36/4
Maximum SH/RH steam temperature, °C	565
Sub-cooling ΔT, °C	5
Pressure losses in HP/LP economizers, % of inlet pressure	25
Pressure losses in superheaters/reheaters, % of inlet pressure	7/8
Condensing pressure, bar	0.048
HP/IP pumps hydraulic efficiency, %	85/75
HP/IP/LP steam turbine isentropic efficiency, %	92/94/88
Turbine mechanical efficiency, %	99.6
Electric generator efficiency, %	98.7
CO_2 compression and purification	
HT/HL knock-out drum separation temperature, °C	−33/−54
Drier inlet pressure, bar	25.8

Table 2 (*Continued*)

Minimum ΔT in heat exchangers, °C	2
Expanders isentropic/mechanical-electric efficiency, %	82/90
Expanders inter-heaters outlet temperature, °C	−45
IC compressor isentropic/mechanical-electric efficiency, %	82/94
Last stage IC compressor CO_2 discharge pressure, bar	88
Intercoolers outlet temperature, °C	30
CO_2 condensation temperature, °C	25
Pressure drop in each intercooler, % of inlet pressure	1
Pump mechanical efficiency, %	90
Pump hydraulic efficiency, %	75
CO_2 delivery pressure, bar	150
Other auxiliaries	
Power for heat rejection to the environment, MJ_e/MJ_{th}	0.008
Miscellaneous balance of plant, % of input coal LHV	0.15

[a] Values in the table are referred to large machines: the actual efficiency is calculated by GS code as function of the machine/stage size.

reaction. This process continues until the oxygen carrier becomes completely oxidized and the outlet mass flow rate increases to equal the inlet mass flow rate. After this point, no reactions take place and the temperature starts dropping due to heat extraction by the air stream.

The significant variations in the red shaded area of Fig. 3 (the part of the stream that will go to the gas turbine) will not allow for safe and efficient turbine operation. This is why it is important to mix the streams of all the reactors residing in the air stage together in order to minimize these variations. The result of this mixing is shown in Fig. 4 where it can be seen that significant fluctuations still exist, but that these fluctuations are small relative to the total mass flow rate and temperature. In this case, the difference between minimum and maximum values of the dimensionless mass flow rate (Eq. (5)) was only 3.26% of its average, while maximum temperature variation was about 4 °C.

Even though the combined outlet streams from the large cluster of reactors in Case A1 creates a suitable feed stream to the turbine, the short fuel stage time (only 2 min) creates a situation where the time of CO_2 and N_2 mixing becomes relatively long. This is illustrated in Fig. 5 where it becomes clear that the time where significant amounts of CO_2 and N_2 are present simultaneously in the outlet stream is relatively long. This will impede the CO_2 separation efficiency of this process.

Another important insight from Fig. 5 is that the outlet stream composition change is delayed for about 13 s following the change of inlet gasses. This implies that it will also be best to delay the outlet switching mechanism for 13 s relative to the inlet switching mechanism as illustrated in Fig. 5. For Case A1, this will be possible because Fig. 3 shows that the mass flow rate in the first part of the fuel stage is similar to the mass flow rate in the air stage, implying that a blend of the delayed gas turbine stream will show similarly small fluctuations as illustrated in Fig. 4. In fact, the delayed switching case resulted in dimensionless mass flow rate variations of 3.45% and temperature variations of 3.3 °C.

For the other two cases (A2 and A3), however, the mass flow rate in the fuel stage is much lower and the number of reactors from which the outlet streams can be mixed is also lower. This implies that a delayed outlet stream switch will create unacceptably large fluctuations in the mass flow rate to be sent to the turbine. For example, in Case A2 an outlet stream switch at the same time as the inlet stream switch results in a dimensionless mass flow rate variation of 7.87%, while a delayed outlet stream switch results in a variations of about 22%. For Case A3, these values were 25% and 96% respectively.

The outlet switch delay which could be accomplished in Case A1 resulted in significant increases in CO_2 separation performance. The CO_2 separation efficiency (percentage of produced CO_2 not lost through the stream going to the gas turbine) increases from 85.9% to 89.9%, while the CO_2 purity (the percentage of CO_2 in the stream going to CO_2 compression after steam condensation) increased from 78.5 to 84.8%. When no outlet switch delay was implemented, the other two cases achieved very similar CO_2 separation performance as Case A1. These results together with the lower total number of reactors imply that a large reactor cluster similar to Case A1, with similar air and fuel feed flow rates to the reactors, appears as the best configuration. There-fore, this configuration will be employed in the remainder of this work.

4.2. Effect of oxygen carrier utilization

The runs completed in the previous section have a fairly low oxygen carrier utilization of around 22.5% in order to limit the

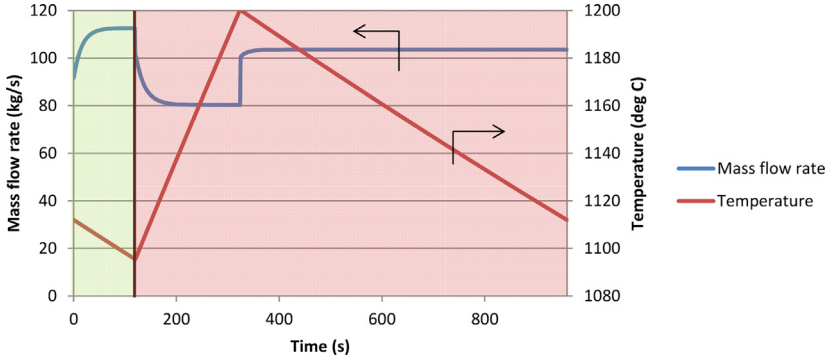

Fig. 3. Reactor outlet mass flow rate and temperature across the cycle for Case A1. The green shaded area indicates the fuel stage (first 120 s) and the red shaded area indicates the air stage (120–960 s). (For interpretation of the references to colour in this figure legend, the reader is referred to the web version of the article.)

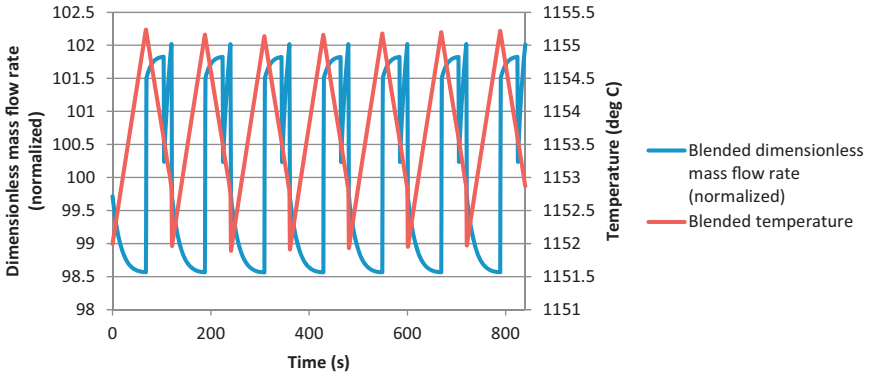

Fig. 4. Dimensionless mass flow rate (Eq. (5)) and temperature of the combined outlet stream of the 8 reactors in the air stage in Case A1. The dimensionless mass flow rate was normalized so that the average value over the cycle was set to a value of 100.

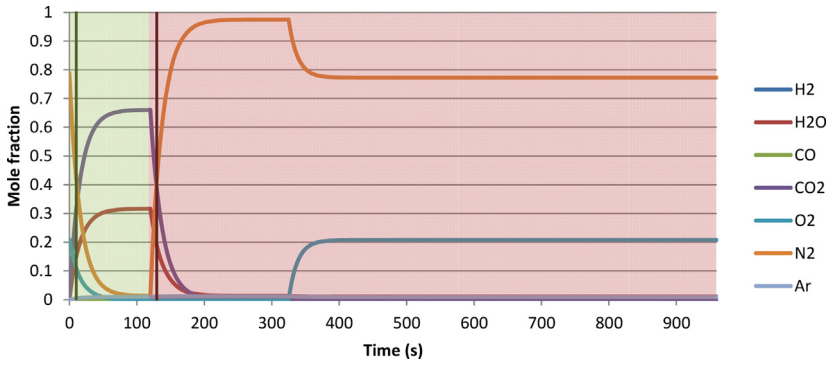

Fig. 5. Reactor outlet species mole fractions across the cycle for Case A1. The green shaded area indicates the fuel stage (first 120 s) and the red shaded area indicates the air stage (120–960 s). The two vertical lines at $t = 13$ s and $t = 133$ s indicate the delay in outlet gas switching necessary to improve CO_2 separation.

Table 3
Stage times and gas feed rates for the simulations investigating the effect of fuel feed rate.

Case	Fuel feed rate (kg/s)	Air feed rate (kg/s)	Fuel stage time (s)	Air stage time (s)
A1	72.27	103.7	120	840
A2	30.97	103.7	280	840
A3	10.32	103.7	840	840

temperature variation across the cycle. The greater temperature variation occurring at higher levels of oxygen carrier utilization would be thermodynamically unfavourable, but will also reduce the length of the CO_2/N_2 mixing periods between oxidation and reduction relative to the total cycle length, thereby improving the CO_2 separation efficiency. This trade-off will be investigated more closely in this section through the cases outlined in Table 4. Note that Case B1 is identical to Case A1 in Table 3.

In Fig. 6, the performance of the GSC process for the four Cases B1–B4 (identified by the maximum OC utilization) is reported in terms of N_2 stream temperature, CO_2 purity and CO_2 separation efficiency. Values of CO_2 purity and CO_2 separation efficiency in this case refer only to the GSC system (i.e. they are different from the overall values of the complete plant). In Fig. 7, the resulting electric efficiency and CO_2 capture ratio obtained by the complete power plant simulations are reported.

First, it can be observed that by increasing the OC utilization from 22.8 to 91.2%, the average temperature of the N_2 stream reduces from about 1154 °C to 965 °C (Fig. 6). This is due to the higher temperature increase during the air stage when OC utilization is increased, as a consequence of the longer duration of the oxidation reactions and the upper temperature limit of 1200 °C assumed.

The lower turbine inlet temperature has a direct effect on the power plant efficiency, which reduces by about 5.5 percentage points in the range assessed (Fig. 7). On the other hand, low OC utilizations lead to larger gas mixing when reactor feeding is switched from air to fuel stage and vice versa. As shown in Fig. 6, this leads

Table 4
Stage times and air feed rates for the simulations investigating the effect of oxygen carrier utilization. The fuel feed rate was kept constant at 72.27 kg/s for all cases. The maximum OC utilization indicates the degree of conversion that would be achieved if 100% of the fuel feed reacted successfully.

Case	Maximum OC utilization (%)	Air feed rate (kg/s)	Fuel stage time (s)	Air stage time (s)
B1	22.8	103.7	120	840
B2	45.6	100.5	240	1920
B3	68.4	102.0	360	3240
B4	91.2	98.0	480	5280

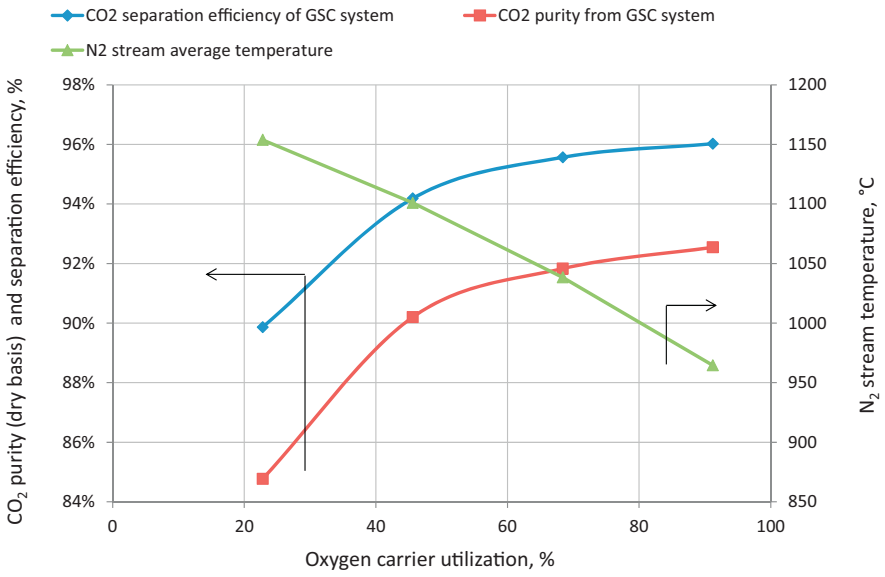

Fig. 6. Performance of the GSC process for different OC utilizations, in terms of N_2 temperature, CO_2 purity and CO_2 separation efficiency.

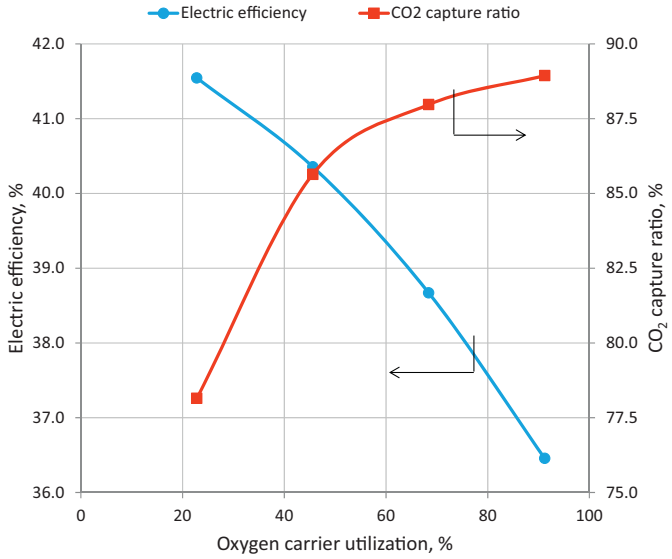

Fig. 7. Power cycle performance in terms of electric efficiency and CO_2 capture ratio for the different oxygen carrier utilization cases.

to both lower CO_2 separation efficiencies (due to CO_2 slip to the N_2 stream) and lower CO_2 purities (due to N_2 and O_2 slip to the CO_2 stream). The same trend is observed for the overall CO_2 capture ratio from the complete plant (Fig. 7). Values of the CO_2 capture ratio are however lower than obtained for the sole GSC process. This is due to two additional sources of CO_2 losses: CO_2 leakage from the CPU (primarily influenced by the purity of the CO_2-rich stream and hence by the operation of the GSC process) and CO_2 emissions from the lock-hoppers and coal drying system (inherent to the coal gasification process and independent of the GSC process). The contributions of these three sources to CO_2 emissions are given in Fig. 8 where it becomes clear that the CO_2 separation efficiency of the reactors is the major factor driving CO_2 emissions from the simulated plant.

4.3. *Effect of steam purging*

An alternative option for improving CO_2 capture efficiency while maintaining reasonable electric efficiencies is to insert a steam

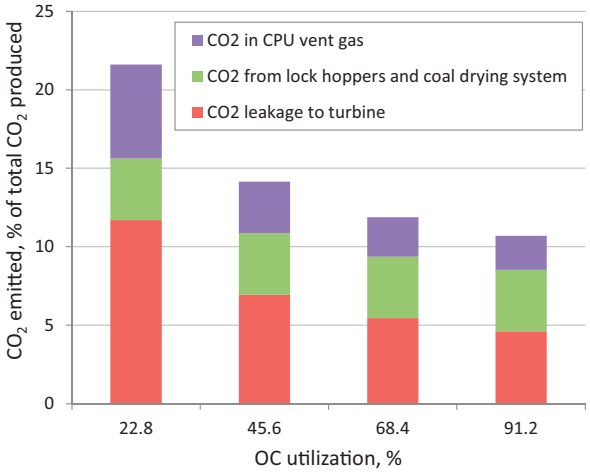

Fig. 8. Sources of CO_2 emission for different oxygen carrier utilizations.

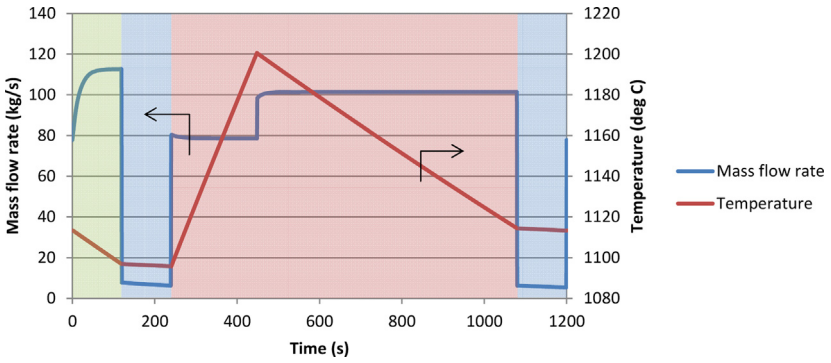

Fig. 9. Reactor outlet flow rate and temperature over the cycle of Case C1 in Table 5. The green area indicates the fuel stage (first 120 s), the blue areas the purging stages (120–240 s and 1080–1200s) and the red area the air stage (240–1080s). (For interpretation of the references to colour in this figure legend, the reader is referred to the web version of the article.)

purge stage between the oxidation and reduction stages. Such a purge stage can greatly reduce contact between N_2 and CO_2 when switching from reduction to oxidation, thereby allowing for low degrees of oxygen carrier utilization (and thereby low temperature variations across the cycle) to be implemented. This option was investigated through the cases shown in Table 5.

Cases C1–C5 were assessed where the amount of steam used for purging varies from 0.5 to 2.5 times the reactor volume. In all the cases, the duration of the purge phase was 120 s and therefore leads to the addition of two reactors to the GSC reactor system. In this analysis, it was assumed that no reverse reaction between the reduced oxygen carrier and steam would result. This should be a reasonable assumption under the low levels of oxygen carrier utilization (~20%) investigated here.

A slight modification to the plant flowsheet shown in Fig. 1 was considered for these cases, consisting in the addition of a LP evaporator on the CO_2-rich stream cooling line. As a matter of fact, due to the increased water content in the CO_2-rich stream from the GSC system when steam purging is performed, a higher thermal power can be recovered at medium temperature from the condensation of this steam. Therefore, the addition of this LP evaporator allows reducing the thermodynamic penalty associated to steam purging.

Due to the low steam flow rates, the delayed switching mechanism discussed around Fig. 5 could not be employed. As shown in Fig. 9, very large variations in the mass flow rate at the reac-tor outlet take place when switching from reduction to purge or from oxidation to purge. This implies that the outlet gasses must be switched at the same time as the inlet gasses in order to avoid large fluctuations in the mass flow rate sent to the turbine.

Even though the outlet gasses had to be switched at the same time, good CO_2 capture efficiency could still be achieved due to the purging stage. On the other hand, steam extraction has a detrimental effect on the plant efficiency, since it reduces the steam expanded in the steam turbine. The effect of increasing steam purge rates on electric efficiency and CO_2 capture ratio is given in Fig. 10. The trade-off between electric efficiency and CO_2 capture ratio is once again clearly visible. When comparing Fig. 10 to Fig. 7, it is shown that higher CO_2 capture ratio can be achieved by steam purging. Over 90% capture can be obtained for steam consumptions

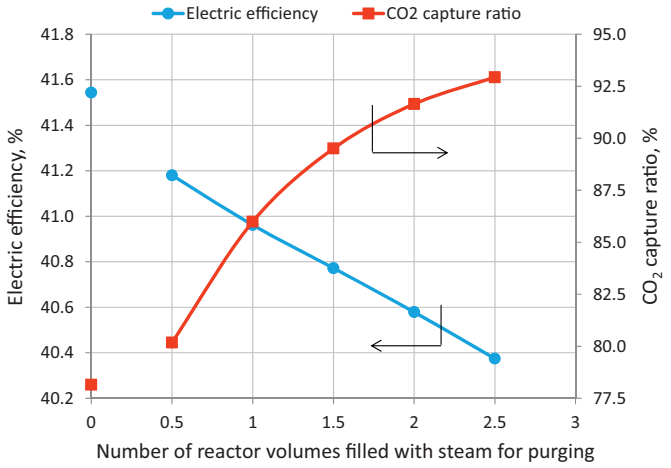

Fig. 10. Power cycle performance in terms of electric efficiency and CO_2 capture ratio for the different steam purging rates. Points with no steam purging (number of reactors filled with steam = 0) are also reported with reference to Case B1.

of about 1.6 reactor volumes per purge step or higher (Fig. 10), to be compared with the 89% reached by simply increasing the OC uti-lization up to 90% (Fig. 7). This result is due to the fact that CO_2 and N_2 mixing can be in principle indefinitely reduced by increasing the steam used for purging. On the contrary, a minimum level of mix-ing between the gases from the different stages is always present by acting only on the OC utilization, related to the volume of the reactors and the amount of reactive gas used in each stage.

From Fig. 10 it is also possible to compare the cases with steam purging with the reference Case B1, without purging (number of reactors filled with steam = 0). As expected, this reference case has higher efficiency and lower CO_2 capture ratio with respect to the cases with purging assessed. It is however evident that its performance would be better than it would be obtained by extrapolating to zero the purging curves. This is due to the favourable effect of the delay switching strategy of Case B1, which would hence perform better than a hypothetical case with very low steam purging.

Table 5
Steam and air feed rates for the simulations investigating the effect of purging. The fuel flow rate was kept at 72.27 kg/s.

Case	Steam flow rate (kg/s)	Air feed rate (kg/s)	Fuel/steam stage time (s)	Air stage time (s)
C1	7.9	101.5	120	840
C2	15.8	99.0	120	840
C3	23.7	97.5	120	840
C4	31.6	95.0	120	840
C5	39.5	93.0	120	840

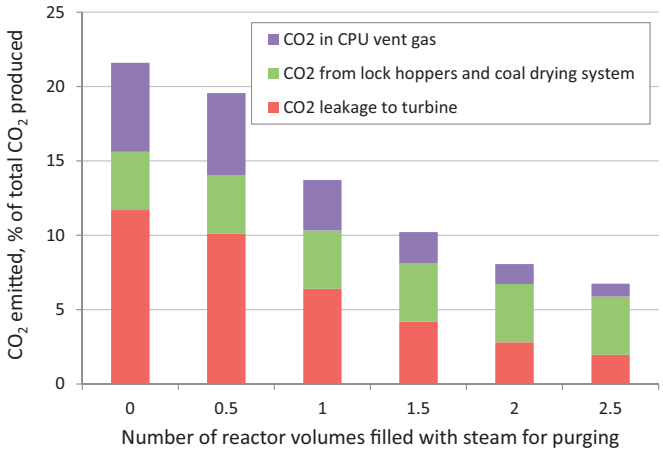

Fig. 11. Sources of CO_2 emission for different steam purging rates.

The breakdown of CO_2 emissions from the cases with different consumption of steam for purge is shown in Fig. 11. The higher reduction of CO_2 leakage to the N_2 stream and of CO_2 lost from the CPU is clear by comparing this figure with Fig. 8.

From the comparison between Fig. 10 and Fig. 7, it also appears that, if intermediate CO_2 capture levels are accepted, the addition of the steam purging step would be slightly preferable over increasing the OC utilization. For example, if a target CO_2 capture ratio of 85 or 80% is selected, net efficiencies of about 40.5 and 41% can be obtained by acting on the OC utilization (Fig. 7), vs. about 41 and 41.1% by introducing the purge stage (Fig. 10).

Finally, one possible way to further improve the performance of this strategy might be to feed the steam at a sufficiently low flowrate in order to defluidize the reactor. This would lead to fluid-dynamic regime closer to plug flow instead of CSTR for the gas flowing through the reactor, thereby improving the quality of purg-ing for a given steam flow rate. More complex modelling is required to accurately describe this strategy and repetitive defluidization and refluidization of the reactor could lead to some operational challenges.

4.4. Advanced heat management strategies

Finally, some advanced heat management strategies have been investigated where both high efficiencies and high CO_2 capture ratio can be achieved. The core of this strategy is a recycling of the N_2 stream from the gas turbine in order to dilute the air stream fed to the reactor during the oxidation stage. Using this process configuration, the temperature rise under oxidation can be controlled so as to limit the temperature variation over the cycle and allow for high efficiencies even for high levels of oxygen carrier utilization.

The simplest such strategy, termed Case D1, would be to dilute the air feed to the oxidation stage with recycled N_2 from HRSG outlet in such a way that the oxidation reaction proceeds for almost the entire oxidation stage. As shown in Fig. 12, this modifica-tion leads to great reductions in the temperature variation across the cycle with respect to a reference case with the same OC uti-lization (i.e. Case B4) and should therefore result in substantial improvements in plant efficiency. In addition, this configuration allows for the fuel stage to take place at high temperatures, thereby achieving high reaction rates and reducing the risk of CO slip when reaching high degrees of oxygen carrier utilization (see Appendix). The oxygen concentration in the oxidant stream needed to obtain the temperature profile of Case D1 is 5.18 vol.%, which is achieved by recycling about 80% of the N_2-rich gas from the HRSG.

Case D3 in Fig. 12 (advanced N_2 recycle) is to feed undiluted air initially (from 480 to 720 s) in order to reach the maximum reactor operating temperature as soon as possible. The feed is then diluted with nitrogen to obtain a 4.67% O_2 content (from 720 to 3600s) so that the reactor outlet temperature stays constant at the maximum attainable temperature for the majority of the oxidation stage. At the end of this period, air is fed again (from 3600 to 3840s) before the fuel stage. This second air stage allows for a continuous feed from the air compressor. According to this strategy, in the cluster of 8 reactors, one reactor is fed with the fuel, one reactor is fed with air and 6 reactors are fed with diluted air. The complete oper-ation strategy is shown in Table 6. This strategy allows obtaining a temperature plateau at 1200 °C for most of the air stage duration, potentially improving the plant efficiency. On the other hand, addi-tional complications are introduced, since three feed streams must be handled by the valve system, more frequent valve switching is required and, differently from Case D1, two compressors (one for air and one for the diluted air stream) are needed to feed the system. In order to further improve the thermodynamic efficiency of the cycle, the fuel gas stream can be pre-heated to 450 °C so that it causes a smaller temperature drop under the reduction stage. This configuration, termed Case D2, would allow for slightly more dilution of the air stream under oxidation (5.08 vol.% of O_2 content vs. 5.18 vol.% of Case D1), thereby further limiting the tempera-ture variation over the cycle in order to increase plant efficiency. In practice, this case returned a similar temperature profile as Case D1 (simple N_2 recycle) in Fig. 12, but reduced the total temperature variation across the cycle from 73.7 °C to 61.6 °C.

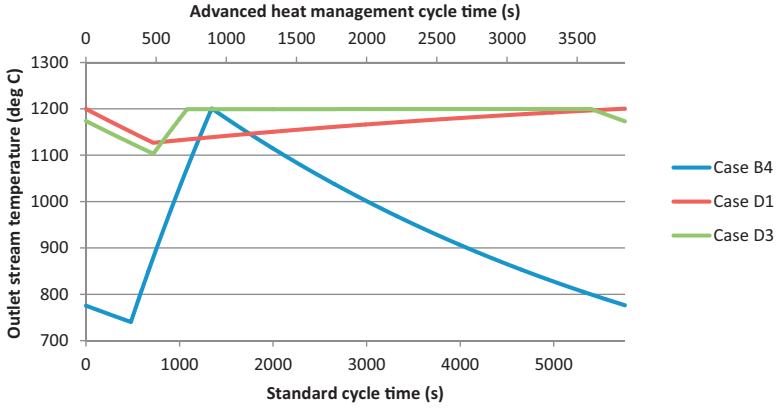

Fig. 12. Comparison of the temperature variation over the standard cycle with a maximum oxygen carrier utilization of 91.2% between Case B4 in Table 4 and two cases with N_2 recycle diluting the air feed stream: simple N_2 recycle (Case D1) and advanced N_2 recycle (Case D3).

Table 6
Operation strategy of the reactor cluster in Case D3 – advanced N_2 recycle (F = fuel stage, A = air feed, DA = diluted air feed).

Time (s)		Reactor	Reactor	Reactor	Reactor	Reactor	Reactor	Reactor	Reactor
from	to	1	2	3	4	5	6	7	8
0	240	F	DA	DA	DA	DA	DA	DA	A
240	480	F	A	DA	DA	DA	DA	DA	DA
480	720	A	F	DA	DA	DA	DA	DA	DA
720	960	DA	F	A	DA	DA	DA	DA	DA
960	1200	DA	A	F	DA	DA	DA	DA	DA
1200	1440	DA	DA	F	A	DA	DA	DA	DA
1440	1680	DA	DA	A	F	DA	DA	DA	DA
1680	1920	DA	DA	DA	F	A	DA	DA	DA
1920	2160	DA	DA	DA	A	F	DA	DA	DA
2160	2400	DA	DA	DA	DA	F	A	DA	DA
2400	2640	DA	DA	DA	DA	A	F	DA	DA
2640	2880	DA	DA	DA	DA	DA	F	A	DA
2880	3120	DA	DA	DA	DA	DA	A	F	DA
3120	3360	DA	DA	DA	DA	DA	DA	F	A
3360	3600	DA	DA	DA	DA	DA	DA	A	F
3600	3840	A	DA	DA	DA	DA	DA	DA	F

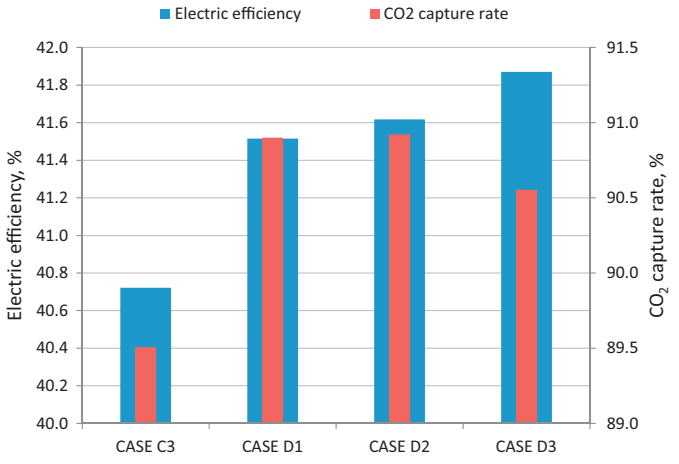

Fig. 13. The effect of advanced heat management through N_2 recycling on plant performance. Cases D1, D2 and D3 represent the simple N_2 recycle, simple N_2 recycle with fuel preheating and advanced N_2 recycle strategies respectively. Case C3 represents a reference case with steam purging with comparable CO_2 capture efficiency.

The performance of these three alternative configurations is compared in Fig. 13 to the case without N_2 recycle but with steam purging characterized by a similar CO_2 capture ratio, approaching 90% (Case C3 in Table 5). It is clear that all cases with advanced heat management showed substantial increases in electric efficiency while maintaining high CO_2 capture ratio. Further improve-ments through fuel preheating or more complex N_2 recycling only offer marginal benefits which may not justify the added complexity.

On the other hand, advantages related to the avoidance of the steam purging step lie in the reduced water consumption of the plant and to the avoidance of two additional reactors dedicated to the purging steps. Such advantages should be balanced with the increased complexity introduced by the N_2 recycle system, considering the economics and the operability of the system.

4.5. Direct performance comparison

In this section, the detailed energy balance for five selected cases is reported and compared with benchmark IGCC plants with and without CO_2 capture. The reference capture technology for IGCCs is physical absorption by Selexol process, which follows a two-stage WGS reactors unit, described for example in Spallina et al.(2014). Following the same approach (Spallina et al., 2014), two gas turbine technologies have been considered for the IGCCs in this study. The first one (advanced GT technology) considers a TIT of 1360 °C, typical of state-of-the-art natural gas-fired machines. The second one (current GT technology) considers more conservative TITs of 1305 °C and 1261 °C for the cases without and with capture respectively, in line with the current practice when a gas turbine designed for natural gas operations is adapted for operations with syngas and hydrogen-based fuel. The global performances of the four benchmark IGCCs are reported in Table 7.

In order to evaluate the performance of the GSC cases, the specific primary energy consumption for CO_2 avoided (SPECCA) index (Eq. (6)) is used. Since two benchmark IGCC technologies have been considered, the SPECCA index has been evaluated as referred to both the current ($SPECCA_{CUR}$) and the advanced ($SPECCA_{ADV}$) gas turbine technology.

$$SPECCA = \frac{((1/\eta_{el}) - (1/\eta_{el,ref}))}{E_{CO_2,ref} - E_{CO_2}} \quad (6)$$

The detailed energy balances of five selected GSC cases are reported in Table 8. In the first three columns, the balance of the Cases B1, B3 and C3 is reported. Case B1 has been selected as benchmark case, while Cases B3 and C3 have been selected from the corresponding set of simulations since they have a CO_2 capture efficiency at least of about 88%. The main difference in the power balance is related to power produced by the steam turbine. Case B1 shows the high-est steam turbine power output, thanks to: (i) the high quality of the heat recovered in the HRSG, consequence of the high temper-ature of the hot gas (due to the high TIT) and (ii) the lack of steam extraction for GSC reactor purging. In Case C3, steam turbine power output reduces by $7MW_e$ due to steam extraction for purging. In Case B3, the minimum steam turbine power is calculated, due to the lowest HP steam production in the HRSG, consequence of the

Table 7
Performance of the reference IGCCs with and without CO_2 capture.

GT technology	Advanced	Current	Advanced	Current
TIT, °C	1360	1261	1360	1261
CO_2 capture	No	No	Yes	Yes
Power balance (MW_e)				
Gas turbine	309.6	261.6	322.5	263.9
Steam turbine	194.6	179.5	184.8	161.2
Auxiliaries	−86.3	−73.8	−120.2	−107.8
Net power, MW_e	417.3	367.4	387.1	317.3
Heat input, MWLHV	882.6	812.5	1026.9	898.7
Net efficiency, %	47.28	45.21	37.70	35.31
CO_2 capture ratio, %	–	–	89.7	89.7
CO_2 emissions, g/kW h	736.0	769.8	96.0	101.4
CO_2 avoided, %	–	–	86.96	86.83
$SPECCA_{CUR}$, $MJ_{LHV/kg_{CO_2}}$	–	–	–	3.34
$SPECCA_{ADV}$, $MJ_{LHV/kg_{CO_2}}$	–	–	3.02	–

low TIT. Since power generated in the gas turbine is similar in these three cases, as well as the power consumed by auxiliaries, steam turbine determines the final efficiency of these plants, which ranges from 38.7 to 41.5%.

As far as CO_2 emissions are concerned, as already discussed Case B1 shows a poor CO_2 capture ratio, below 80%. In Case C3, a good compromise between CO_2 capture ratio (89.5%) and efficiency (40.8%) is obtained, leading to SPECCA of 1.27 and 1.86 MJ_{LHV}/kg_{CO_2} depending on the reference IGCC technology considered. Case B3 appears as a sub-optimal case, having both worse efficiency and worse emissions than Case C3.

If compared to the reference IGCC with CO_2 capture, GSC plants perform generally better than benchmark IGCC technology, which are characterized by SPECCA higher than 3 MJ_{LHV}/kg_{CO_2}. This result is due to the significantly higher efficiency of these GSC cases and could be improved if the emissions associated to the CPU vent were reduced, for example by recovering the CO_2 through commercial VPSA or polymeric membranes systems, as proposed by CPU developers (Shah et al., 2011; White et al., 2013). If such systems are applied, CO_2 capture ratio higher than 90% could be achieved for the GSC Cases B3 and C3.

In the last three columns of Table 8, the balances of the cases with advanced heat management by N_2 recycle are shown (Cases D1–D3). In these cases, the high gas turbine inlet temperature and the lack of steam extraction from the turbine lead to the highest gross power productions and the highest net efficiencies, up to values of 41.6–41.9%. Fuel preheating (Case D2) allows improving the net efficiency by about 0.1 percentage points with respect to Case D1 (from 41.6 to 41.7%). The advanced N_2 recycle system (Case D3) increases the efficiency by 0.35 percentage points with respect to Case D1. Also the specific emissions are highly improved in the cases with advanced heat management system, passing 90% of CO_2

Table 8
Detailed power balance of selected GSC cases.

Case	B1	B3	C3	D1	D2	D3
Maximum oxygen carrier utilization	22.8	68.4	22.8	81.2	81.2	81.2
N. of reactors filled with steam for purge	–	–	1.5	–	–	–
N_2 recycle for heat management	No	No	No	Simple recycle	Simple recycle	Advanced recycle
Syngas preheating temperature, °C	300	300	300	300	450	300
Gas turbine inlet temperature, °C	1154	1038	1155	1168	1173	1196
Power balance, MW_e						
Gas turbine	194.6	197.0	196.2	187.7	193.0	190.6
Steam turbine	221.0	194.6	213.5	229.0	224.4	229.0
Steam cycle pumps	−4.43	−4.30	−4.52	−4.59	−4.47	−4.61
Auxiliaries for heat rejection	−3.57	−3.63	−3.64	−3.69	−3.66	−3.68
ASU	−33.84	−33.84	−33.84	−33.84	−33.84	−33.84
CO_2 compression (including l-h)	−13.10	−13.54	−13.59	−13.63	−13.65	−13.49
N_2 compressor	−1.36	−1.36	−1.36	−1.36	−1.36	−1.36
Syngas recycle fan	−1.00	−1.00	−1.00	−1.00	−1.00	−1.00
Coal milling and handling	−1.60	−1.60	−1.60	−1.60	−1.60	−1.60
Ash handling	−0.48	−0.48	−0.48	−0.48	−0.48	−0.48
Acid gas removal	−0.36	−0.36	−0.36	−0.36	−0.36	−0.36
BOP	−1.28	−1.28	−1.28	−1.28	−1.28	−1.28
Gross power, MW_e	415.7	391.5	409.7	416.7	417.4	419.6
Net power, MW_e	354.6	330.1	348.1	354.9	355.7	357.9
Heat input, MW_{LHV}	853.7	853.7	853.7	853.7	853.7	853.7
Net efficiency, %	41.54	38.67	40.77	41.57	41.67	41.92
CO_2 capture ratio, %	78.15	87.97	89.51	90.90	90.92	90.55
CO_2 emissions, g/kW h	178.7	103.4	84.2	71.4	71.0	73.1
CO_2 avoided, %	76.8	86.6	89.1	90.7	90.8	90.5
$SPECCA_{CUR}$, MJ_{LHV}/kg_{CO2}	1.19	2.02	1.27	1.00	0.97	0.90
$SPECCA_{ADV}$, MJ_{LHV}/kg_{CO2}	1.89	2.68	1.86	1.57	1.54	1.47
Sources of CO_2 emission, g/kW h						
CO_2 vented from CPU	49.6	21.9	17.5	14.6	14.8	12.8
Other sources (lock hoppers, syngas drying)	32.5	34.1	32.3	32.9	32.8	32.6
CO_2 leakage to N_2 stream	96.9	47.5	34.5	24.0	23.5	27.8

avoided. As a result, remarkable $SPECCA_{CUR}$ and $SPECCA_{ADV}$ values of 0.90–1.00 and 1.47–1.57 are obtained.

If compared to other integrated gasification CLC power plants based on packed bed or fluidized bed reactor systems, somewhat lower efficiencies and higher emissions have been obtained for the GSC processes with standard heat management system. However, if N_2 recycle is adopted, efficiency passes by 0.5–0.8 percentage points the best packed bed case calculated in Spallina et al. (2014) using ilmenite as oxygen carrier, by 0.1–0.8 percentage points the packed bed and fluidized bed reactors cases with Nickel as OC reported in Hamers et al. (2014) and by 0.7–1.1 percentage points the best two-stage packed bed case described in Hamers et al. (2015). On the other side, mainly due to the gas leakages when switching GSC reactors from air to fuel feed and vice versa, the specific emissions of the GSC cases are significantly higher than in packed bed and fluidized bed systems in those works. As already commented, such values could be partly reduced by limiting the emissions from the CPU by integrating commercial CO_2 recovery systems. Assessing advanced reactor design or more sophisticated operation strategies limiting such unwanted leakages would also contribute in further improving the potential of the GSC process.

5. Summary and conclusions

This paper assesses the thermodynamic performance of a power plant using the new concept of Gas Switching Combustion (GSC) with syngas from coal gasification as fuel. The GSC concept offers a simpler and more scalable alternative to the standard Chemical Looping Combustion (CLC) concept for power production with integrated CO_2 capture. In particular, the substantial operational and scale-up challenges brought by the need for circulating solids between two reactors are completely eliminated by keeping the oxygen carrier material inside of a single reactor where it is alternatively exposed to oxidative and reductive conditions.

Due to the transient nature of the GSC concept, a cluster of reactors is required to supply two steady gas streams to a downstream gas turbine and CO_2 purification and compression units. It was shown that mixed streams from such a cluster of reactors could supply a high pressure stream to a gas turbine with sufficiently small fluctuations in temperature and mass flow rate.

Various operating strategies were investigated for the GSC concept. In the simplest configuration where fuel and air streams are simply fed alternatively to the reactor, the degree of oxygen carrier utilization is the most important controlling parameter. Lower degrees of oxygen carrier conversion in each cycle resulted in higher thermal efficiencies and lower degrees of CO_2 avoidance, and vice versa for high degrees of oxygen carrier conversion. A lower degree of oxygen carrier conversion not only will reduce the degree of temperature variation over the cycle, thereby allowing for a higher average operating temperature (thus increasing the electric efficiency), but will also cause the time of undesired mixing of CO_2 and N_2 right after a switch in the inlet gasses to increase relative to the total cycle time (thus reducing the CO_2 avoidance).

Introducing a steam purging stage between the air and fuel stages resulted in moderate improvements in CO_2 avoidance for a given electric efficiency. However, the best overall performance in terms of electric efficiency and CO_2 avoidance could be achieved through advanced heat management strategies where an N_2 recycle stream is used to limit the overall temperature variation over longer cycles featuring a high degree of oxygen carrier utilization. Further studies are required to determine whether the increased performance achieved by the advanced heat management strategies justifies the increase in process complexity.

Finally, the performance of different configurations of the GSC concept was compared to two baseline IGCC plants with currently available CO_2 capture technology. The simplest GSC configuration achieved a significantly higher electric efficiency (41.5%) than the baseline IGCC cases using current (35.3%) and advanced (37.7%) gas turbine technology while avoiding about 10 percentage points less CO_2. Inclusion of an H_2O purge stage between fuel and air feeds could improve CO_2 avoidance (2 percentage points higher than the baseline IGCC) by keeping a significantly higher electric effi-ciency (+3.0–5.4 percentage points). Advanced heat management achieved thermal efficiencies as high as 41.9% while avoiding about 3.5 percentage points more CO_2 than the baseline cases. The GSC concept therefore appears to offer a promising pathway for accelerating the development process of CLC-based technology.

Acknowledgement

The authors gratefully acknowledge the financial support from SINTEF Materials and Chemistry under the POP-SEP grant.

Appendix: Complete fuel conversion assumption.

The CSTR model described in Section 2.1 makes an important assumption in the form of complete gaseous reactant conversion as long as all necessary reactants are present. This assumption could potentially lead to significant errors in certain cases, particularly when it comes to CO conversion towards the end of the reduction stage when long cycle times are considered (e.g. Case B4 in Table 4). At the end of the reduction stage, the reaction rate reduces for two reasons: (1) this is the lowest temperature point in the cycle and(2) the oxygen carrier is at its highest degree of reduction.

The reduction of Fe_2O_3 to FeO by CO is typically the slowest reaction taking place in this system, especially at lower temperatures. This reaction will therefore be the subject of this section. A typical rate equation for this reaction is shown below applying the shrinking unreacted core model with reaction rate control (Levenspiel, 1999) on microscopic grains (d_{gr} = 2.5 μm) inside each particle:

$$R_H = -\frac{dC_{CO}}{dt} = \frac{6}{d_{gr}} s_{Fe_2O_3} \alpha_s k_{CO} C_{CO}^n \tag{7}$$

Here, $s_{Fe_2O_3}$ is the fraction of the surface area of the unreacted core of each grain relative to the surface area of the grain itself (the surface area of the unreacted core when the particle is fully oxidized). It is approximated based on the degree of conversion of the oxygen carrier as follows:

$$s_{Fe_2O_3} \approx \left(\frac{2y_{Fe_2O_3}}{2y_{Fe_2O_3} + y_{FeO}} \right)^{2/3} \tag{8}$$

The reaction rate constant for this reaction is given below (Abad et al., 2011), noting that the reaction order is 0.8:

$$k_{CO} = 0.1e^{(-80700/RT)} \tag{9}$$

The surface area for reaction (Eq. (8)) and the reaction rate constant (Eq. (9)) will change during the reduction stage of the GSC process. As an example, the effective reaction rate constant (Eq. (10)) is plotted along the fuel stage of Case B4 in Table 4 in Fig. 14.

$$k_{eff,CO} = \frac{6}{d_{gr}} s_{Fe_2O_3} k_{CO} \tag{10}$$

It is clear that the effective reaction rate constant reduces by an order of magnitude over the course of the fuel stage, primarily as a result of a reduction of the available active surface area on the grains (Eq. (8)) as they become more converted. To get a broader overview, the effective reaction rate constant is plotted at the end of the reduction stage for all the cases investigated in Sections 4.2 and 4.4 in Fig. 15.

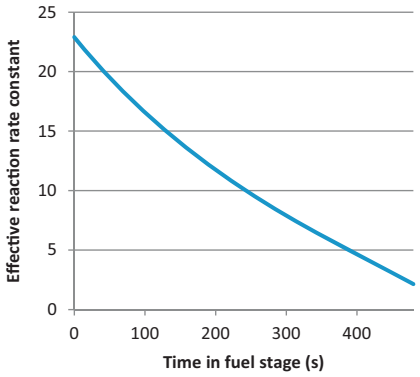

Fig. 14. Evolution of the effective reaction rate constant along the fuel stage of Case B4 in Table 4.

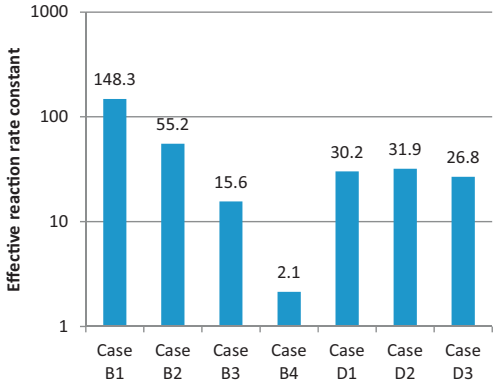

Fig. 15. Effective reaction rate at the end of the reduction stage for different cases evaluated in this study.

The results show that reaction kinetics at the end of the reduction stage in Case B4 is much slower than for any other case. Performance of the reactor with this kinetics can be simply assessed by solving the following species conservation equation along the height (x) of the reactor:

$$-U_g \frac{dC_{CO}}{dx} = R_H \tag{11}$$

When solving this equation by substituting in Eq. (7), the CO mole fraction along the height of the reactor can be obtained (assuming a solids volume fraction of 0.35 throughout the reactor volume). Fig. 16 shows the result for the kinetic rate as well as three additional cases with slower kinetics. It is shown that the assumption of complete conversion will hold as long as mass transfer limitations in the reactor do not decrease the reaction rate by more than a factor of four (which is unlikely given the low reaction rate). When considering the effective reaction rate constants in Fig. 15, it is clear that complete conversion will be easily achieved for all other cases evaluated in this work.

One possible effect which could make the assumption of complete conversion invalid for Case B4 is a large reduction in the reaction rate constant with increasing system pressure. An inversely proportional relationship between the reaction rate constant and the system pressure was found for an Fe-based oxygen carrier material (Abad et al., 2007), but this relationship has not yet been investigated for ilmenite.

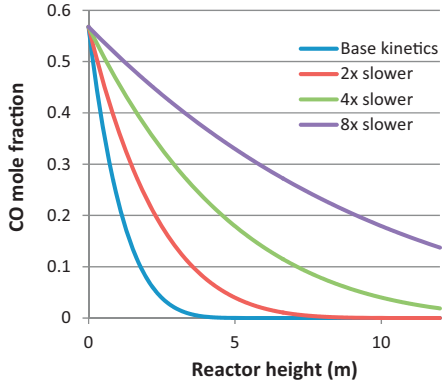

Fig. 16. CO mole fractions along the height of the reactor for different kinetics, with an OC utilization of 91.4% (end of the reduction stage in Case B4).

References

Abad, A., Adánez, J., Cuadrat, A., García-Labiano, F., Gayán, P., de Diego, L.F., 2011. Kinetics of redox reactions of ilmenite for chemical-looping combustion. Chem. Eng. Sci. 66, 689–702.

Abad, A., Adánez, J., García-Labiano, F., de Diego, L.F., Gayán, P., Celaya, J., 2007. Mapping of the range of operational conditions for Cu-, Fe-, and Ni-based oxygen carriers in chemical-looping combustion. Chem. Eng. Sci. 62, 533–549.

Adanez, J., Abad, A., Garcia-Labiano, F., Gayan, P., de Diego, L.F., 2012. Progress in chemical-looping combustion and reforming technologies. Prog. Energy Combust. Sci. 38, 215–282.

Adanez, J., Cuadrat, A., Abad, A., Gayan, P., Diego, L.F.D., Garcia-Labiano, F., 2010. Ilmenite activation during consecutive redox cycles in chemical-looping combustion. Energy Fuels 24, 1402–1413.

Brandvoll, Bolland, O., 2004. Inherent CO_2 capture using chemical looping combustion in a natural gas fired power cycle. J. Eng. Gas Turbines Power 126, 316–321.

Chiesa, P., Campanari, S., Manzolini, G., 2011. CO_2 cryogenic separation from combined cycles integrated with molten carbonate fuel cells. Int. J. Hydrogen Energy 36, 10355–10365.

Consonni, S., Rossini, S., Saviano, F., Lozza, G., Pelliccia, G., 2006. Chemical-looping combustion for combined cycles with CO_2 capture. J. Eng. Gas Turbines Power 128, 525–534.

Cormos, C.-C., 2010. Evaluation of iron based chemical looping for hydrogen and electricity co-production by gasification process with carbon capture and storage. Int. J. Hydrogen Energy 35, 2278–2289.

Cuadrat, A., Abad, A., Adánez, J., de Diego, L.F., García-Labiano, F., Gayán, P., 2012. Behavior of ilmenite as oxygen carrier in chemical-looping combustion. Fuel Process. Technol. 94, 101–112.

DemoCLOCK, 2011. www.sintef.no/Projectweb/DemoClock/

EBTF, 2011. European best practice guide for assessment of CO_2 capture technologies. European Benchmark Task Force.

Erlach, B., Schmidt, M., Tsatsaronis, G., 2011. Comparison of carbon capture IGCC with pre-combustion decarbonisation and with chemical-looping combustion. Energy 36, 3804–3815.

Gecos, 2014. GS Software. www.gecos.polimi.it/software/gs.php

Hamers, H.P., Gallucci, F., Cobden, P.D., Kimball, E., van Sint Annaland, M., 2013. A novel reactor configuration for packed bed chemical-looping combustion of syngas. Int. J. Greenh. Gas Control 16, 1–12.

Hamers, H.P., Romano, M.C., Spallina, V., Chiesa, P., Gallucci, F., van Sint Annaland, M., 2014. Comparison on process efficiency for CLC of syngas operated in packed bed and fluidized bed reactors. Int. J. Greenh. Gas Control 28, 65–78.

Hamers, H.P., Romano, M.C., Spallina, V., Chiesa, P., Gallucci, F., Van Sint Annaland, M., 2015. Energy analysis of two stage packed-bed chemical looping combustion configurations for integrated gasification combined cycles. Energy 85, 489–502.

Hiby, J.W., 1964. Untersuchungen über den kritischen Mindestdruckverlust des Anströmbodens bei Fluidalbetten (Fließbetten). Chem. Ing. Tech. 36, 228–229.

Håkonsen, S.F., Blom, R., 2011. Chemical looping combustion in a rotating bed reactor – finding optimal process conditions for prototype reactor. Environ. Sci. Technol. 45, 9619–9626.

Håkonsen, S.F., Grande, C.A., Blom, R., 2014. Rotating bed reactor for CLC: bed characteristics dependencies on internal gas mixing. Appl. Energy 113, 1952–1957.

IEA, 2005. Oxy Combustion Processes for CO_2 Capture from Power Plant, IEA Report 2005/9. IEA Greenhouse Gas R&D Programme.

Kunii, D., Levenspiel, O., 1991. Fluidizaton Engineering, 2nd ed. utterworth-Heinemann (Chapter 4).

Levenspiel, O., 1999. Chemical Reaction Engineering, 3rd ed. John Wiley & Sons, United States.

Lozza, G., Chiesa, P., Romano, M.C., Savoldelli, P., 2006. Three reactors chemical looping combustion for high efficiency electricity generation with CO_2 capture from natural gas. In: ASME Turbo Expo 2006.

Lyngfelt, A., 2014. Chemical-looping combustion of solid fuels – status of development. Appl. Energy 113, 1869–1873.

Naqvi, R., Bolland, O., 2007. Multi-stage chemical looping combustion (CLC) for combined cycles with CO_2 capture. Int. J. Greenh. Gas Control 1, 19–30.

Naqvi, R., Wolf, J., Bolland, O., 2007. Part-load analysis of a chemical looping combustion (CLC) combined cycle with CO_2 capture. Energy 32, 360–370.

Noorman, S., Gallucci, F., van Sint Annaland, M., Kuipers, J.A.M., 2011a. Experimental investigation of chemical-looping combustion in packed beds: a parametric study. Ind. Eng. Chem. Res. 50, 1968–1980.

Noorman, S., Gallucci, F., van Sint Annaland, M., Kuipers, J.A.M., 2011b. A theoretical investigation of CLC in packed beds. Part 2: reactor model. Chem. Eng. J. 167, 369–376.

Ortiz, M., Gallucci, F., Snijkers, F., Van Noyen, J., Louradour, E., Tournigant, D., van Sint Annaland, M., 2014. Development and testing of ilmenite granules for packed bed chemical-looping combustion. Chem. Eng. J. 245, 228–240.

Robie, R., Hemingway, B.,1995. Thermodynamic properties of minerals and related substances at 298.15 K and 1 bar pressure and at higher temperatures. In: Interior. U.S.D.o.t.

Shah, M., Degenstein, N., Zanfir, M., Kumar, R., Bugayong, J., Burgers, K., 2011. Near zero emissions oxy-combustion CO_2 purification technology. In: 10th International Conference on Greenhouse Gas Control Technologies, September 19, 2010–September 23, 2010. Elsevier Ltd, Amsterdam, Netherlands, pp. 988–995.

Sorgenfrei, M., Tsatsaronis, G., 2014. Design and evaluation of an IGCC power plant using iron-based syngas chemical-looping (SCL) combustion. Appl. Energy 113, 1958–1964.

Spallina, V., Gallucci, F., Romano, M.C., Chiesa, P., Lozza, G., van Sint Annaland, M., 2013. Investigation of heat management for CLC of syngas in packed bed reactors. Chem. Eng. J. 225, 174–191.

Spallina, V., Romano, M.C., Chiesa, P., Gallucci, F., van Sint Annaland, M., Lozza, G., 2014. Integration of coal gasification and packed bed CLC for high efficiency and near-zero emission power generation. Int. J. Greenh. Gas Control 27, 28–41.

Stull, D.R., Prophet, H., 1971. JANAF thermochemical tables. In: Standards, 2nd ed. U.S.N.B.o., Washington, DC.

White, V., Wright, A., Tappe, S., Yan, J., 2013. The air products Vattenfall oxyfuel CO_2 compression and purification pilot plant at Schwarze Pumpe. Energy Procedia 37, 1490–1499.

Wolf, J., Anheden, M., Yan, J., 2005. Comparison of nickel- and iron-based oxygen carriers in chemical looping combustion for CO_2 capture in power generation. Fuel 84, 993–1006.

Zaabout, A., Cloete, S., Johansen, S.T., van Sint Annaland, M., Gallucci, F., Amini, S., 2013. Experimental demonstration of a novel gas switching combustion reactor for power production with integrated CO_2 capture. Ind. Eng. Chem. Res. 52, 14241–14250.